

- 1 Title page
- 2 Title: The Role of Efferent Reflexes in the Efficient Encoding of Speech by the Auditory Nerve
- 3 Abbreviated title: efferent reflexes in efficient encoding of speech
- 4 Authors: Jacques Grange, Mengchao Zhang (张梦超), John Culling
- 5 Affiliation: School of Psychology, Cardiff University, United Kingdom, CF10 3AT
- 6 Corresponding author: grangeja@cardiff.ac.uk
- 7 Number of pages: 33
- 8 Number of figures: 7
- 9 Number of tables: 2
- 10 Number of words for abstract: 232
- 11 Number of words for introduction: 701
- 12 Number of words for discussion: 1450
- 13 Conflict of interest statement: the authors declare no competing financial interests.
- 14 Acknowledgments: This research was funded by an EPSRC project grant (Grant No.:
- 15 EP/R010722/1; P.I.: John Culling).
- 16

17 **ABSTRACT**

18 To avoid information loss, the auditory system must adapt the broad dynamic range of
19 natural sounds to the restricted dynamic range of auditory nerve fibers. How it solves this
20 dynamic range problem is not fully understood. Recent electrophysiological studies showed that
21 dynamic-range adaptation occurs at the auditory-nerve level, but the amount of adaptation found
22 was insufficient to prevent information loss. We used the physiological MATLAB® Auditory
23 Periphery model to study the contribution of efferent reflexes to dynamic range adaptation.
24 Simulating the healthy human auditory periphery provided adaptation predictions that suggest
25 that the acoustic reflex shifts rate-level functions towards a given context level and the medial
26 olivo-cochlear reflex sharpens the response of nerve fibers around that context level. A simulator
27 of hearing was created to decode model-predicted firing of the auditory nerve back into an
28 acoustic signal, for use in psychophysical tasks. Speech reception thresholds in noise obtained
29 with a normal-hearing implementation of the simulator were just 1 dB above those measured
30 with unprocessed stimuli. This result validates the simulator for speech stimuli. Disabling
31 efferent reflexes elevated thresholds by 4 dB, reaching thresholds found in mild-to-moderately
32 hearing-impaired individuals. Overall, our studies suggest that efferent reflexes may contribute
33 to overcoming the dynamic range problem. Because specific sensorineural pathologies can be
34 inserted in the model, the simulator can be used to obtain the psychophysical signatures of each
35 pathology, thereby laying a path to differential diagnosis.

36

37

38 **SIGNIFICANCE STATEMENT**

39 The saturation of auditory nerve fibers at moderate sound levels seen in rate-level
40 functions challenges our understanding of how sounds of wide dynamic range are encoded. Our
41 physiologically inspired simulations suggest that efferent reflexes may play a major role in
42 dynamic range adaptation, with the acoustic reflex moving auditory-nerve rate level function
43 towards a given context level and the medial olivocochlear reflex increasing fiber sensitivity
44 around that context level. A psychophysical task employing advanced simulations showed how
45 the existence of the efferent system could prevent unrecoverable information loss and severe
46 impairment of speech-in-noise intelligibility. These findings illustrate how important the precise
47 modeling of peripheral compression is to both simulations and understanding of normal and
48 impaired hearing.

49 **INTRODUCTION**

50 The dynamic range of an auditory neuron is the portion of its rate-level function (RLF),
51 where its firing rate increases with the input level. Most sounds important to humans, such as
52 speech and music, are highly modulated in amplitude by nature. Changes in firing rate, combined
53 with frequency tuning, is the most straightforward mechanism by which these spectro-temporal
54 modulations in the stimulus might be encoded on the auditory nerve (AN). However, traditional
55 physiological measurements of AN rate-level functions (RLFs) indicate that most AN fibers are
56 already saturated at moderate sound levels (Liberman, 1978; Winter et al., 1990), prompting
57 some researchers to look for alternative codes based on phase-locking, such as the average,
58 localized synchronized rate (Young and Sachs, 1979). Such a timing mechanism, now known to
59 be essential for firing-rate cues at the cortical levels, seemed to be the only way to explain why

60 mammals can continue to process spectral information over a wide dynamic range while AN
61 fibers become saturated. However, recent work has suggested that processes of adaptation lead to
62 a shift of the dynamic range of AN fibers in response to the prevailing sound level in the
63 environment (termed ‘dynamic range adaptation’, DRA), potentially providing a degree of
64 reprieve for firing-rate mechanisms.

65 Wen et al. (2009) showed such DRA in AN fibers of Cat. As seen in early
66 electrophysiological studies, classical firing-rate adaptation is a decrease in firing rate to a steady
67 tone or repeated stimulation (Kiang et al., 1965; Smith and Zwislocki, 1975; Harris and Dallos,
68 1979; Smith, 1979; Chimento and Schreiner, 1991). The RLF shows proportional reductions in
69 firing rate at all stimulus levels. In contrast, DRA is defined as a horizontal shift of RLFs toward
70 the sound levels with the highest frequency of occurrence. Somewhat stronger DRA is seen in
71 the inferior colliculus (Dean et al., 2005) and auditory cortex (Watkins and Barbour, 2008). By
72 shifting RLFs so that AN fibers respond best around the context level, DRA enables fibers to
73 encode short-term amplitude changes with variations in response rate across a wide range of
74 sound levels without saturation. The absence of such adaptation is thus expected to weaken an
75 individual’s ability to process normal-level speech in noise.

76 The mechanisms underlying DRA are unclear. Zilany and Carney (2010) used a
77 phenomenological model of the auditory periphery. They showed that such adaptation could be
78 simulated by applying power-law dynamics at the inner haircell/fiber junction, but this
79 mechanism does not have a physiologically known source. Moreover, although Wen et al.
80 showed DRA at the auditory nerve, the amount of RLF shift (about 0.27 dB/dB) was insufficient
81 to prevent fiber saturation at moderate sound levels. Here, we hypothesize that the efferent
82 reflexes in the auditory periphery, the acoustic reflex and medial olivocochlear reflex (MOCR),

83 have the potential to contribute to DRA. The partial or complete anesthesia-related deactivation
84 of efferent reflexes in electrophysiological studies may have led to substantial underestimation of
85 the amount of adaptation that occurs in an awake state.

86 These efferent reflexes seem good candidates for DRA, because they both reduce
87 acoustic sensitivity following mid- to high-level sounds. The acoustic reflex contracts the
88 middle-ear muscles and reduces the amplitude of stapes vibrations transferred to the cochlea oval
89 window for intense sound levels (Hung and Dallos, 1972). The MOCR reduces the displacement
90 of the basilar membrane by reducing cochlear amplification by outer hair-cells from moderate
91 sound levels upwards (Guinan and Gifford, 1988).

92 The current study explores the mechanisms underlying auditory-nerve-level DRA
93 through computational modelling and simulation based on a computer model of the human
94 auditory periphery (Meddis et al., 2013). First, emergent DRA properties of the human model
95 were compared to previous RLF findings in small mammals. The model reveals the distinct role
96 of each efferent reflex, providing a full picture that had previously been partially hidden by
97 anesthesia in electrophysiological studies. Second, a simulator that decodes the modelled
98 auditory-nerve activity back into sound was used to present reconstructions of the stimulus based
99 on the pattern of AN firing to human listeners. Simulations for which the two reflexes were
100 disabled tested how important the reflexes are for speech perception. Human listeners achieved
101 near-normal speech reception thresholds in noise when listening to simulations that included the
102 efferent reflexes.

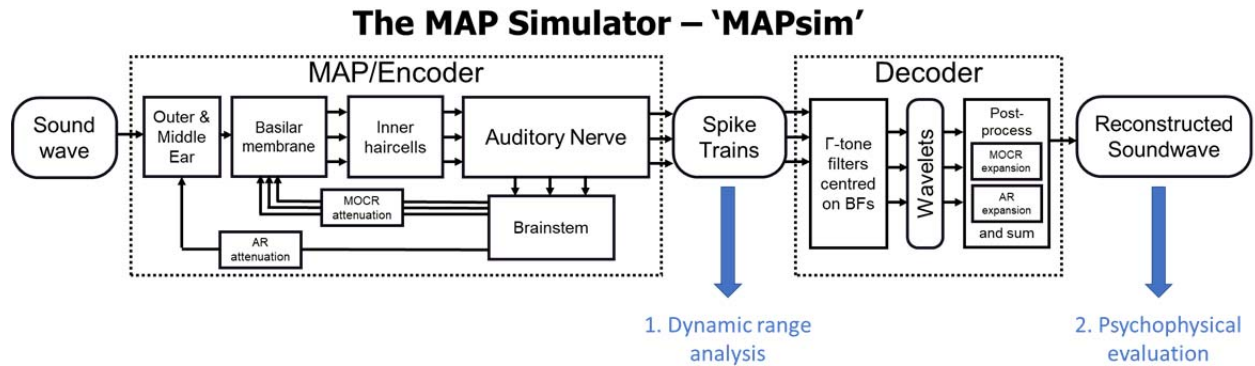
103 **MATERIALS AND METHODS**

104 A simulator of normal and impaired hearing was created, based on the MATLAB[®]
105 Auditory Periphery (MAP) model (Meddis et al., 2013). Coined ‘MAPsim’, the simulator

106 employs two modules (Figure 1). The first module is the MAP model, used to encode stimuli at
107 the auditory nerve level. The second module is a decoder that regenerates an acoustic signal
108 based on MAP-encoded auditory-nerve activity. MAP is used to generate RLF predictions and
109 estimate the contribution of efferent reflexes to DRA. MAPsim is used to simulate normal
110 hearing and illustrate the impact of knocking out efferent reflexes on speech-in-noise
111 intelligibility.

112 *Simulation of auditory nerve activity*

113 The stimuli were encoded into simulated auditory nerve activity using the MAP model.
114 MAP is a physiologically inspired computational model of the auditory periphery with a detailed
115 modular structure that has been parameterized to replicate many physiological and
116 psychophysical data sets (e.g. Panda et al., 2014). As shown in the left-hand section of Figure 1
117 ('MAP/Encoder'), MAP includes: (1) the outer and middle ear filtering, which outputs the stapes
118 displacement, (2) the dual-resonance non-linear (DRNL) model of basilar membrane
119 displacement (Lopez-Poveda and Meddis, 2001), (3) stereocilia flexing and inner hair cell
120 transduction, (4) inner-hair-cell receptor potential, ion currents and neurotransmitter processing,
121 (5) release of neurotransmitter vesicles at the synaptic cleft between inner hair cells and AN
122 fibers, (6) resulting spiking activity of the fibers, (6) two layers of coincidence-detecting
123 MacGregor neurons (MacGregor, 1987) that represent a simplified auditory brainstem network,
124 and (7) the efferent pathways, including a broadband acoustic reflex signal that modulates the
125 stapes displacement and a frequency-specific MOCR signal that differentially modulates the
126 basilar membrane displacement within each best frequency (BF) channel at the DRNL stage.



128

129 *Figure 1. Schematic processing stages of the MAP simulator (MAPsim). Rectangles: signal*
 130 *processing modules of the simulator. Rounded rectangles: input or output signals. One arrow:*
 131 *broadband processing. Three arrows: frequency-specific processing within each BF channel.*
 132 *MAP predicts the AN spike trains of ~30,000 auditory-nerve fibers across 30 BFs and 3 SRs.*

133

134 The closest model implementation to the current study is in Panda et al. (2014). The parameters
 135 to simulate the normal-hearing condition for this study are provided in Table 1. A total of 29,970
 136 AN fibers were arranged over 30 BFs (equally spread on an ERB scale between 56 and 8000 Hz)
 137 and 3 levels (low, medium and high) of spontaneous rate (SR), rendering 333 fibers per BF and
 138 SR combination. The role of efferent reflexes in efficient coding of sound intensity was first
 139 examined through a dynamic range analysis of the encoder.

Module component and Parameter name	Value
OME – Outer & Middle ear - two resonance filters [gain order lowpass highpass (Hz)] high-pass stapes filter [order cut-off frequency (Hz)] air to stapes displacement scalar	[10 1 1000 4000; 25 1 2500 7000] [1 600] 45e-9
Acoustic Reflex - latency and smoothing time constant (ms) low SR stream threshold (spks/s) broadband rate-to-attenuation factor applied to low SR IC firing rate	10 250 40 5e-3
DRNL - number of best frequencies (BFs) frequency range [low high] over which BFs are ERB-spaced (Hz) gain a & compression exponent c compression knee-point (dB relative to ref. displacement) ct non-linear bandwidth parameters [p, q] linear gain g and bandwidth parameters [p, q] linear CFs parameters [p, q] with $CF = p \cdot BF + q$ order of all gammatone filters	30 [56 8000] 6e3 0.25 25 [0.14, 180] 500 [0.2,235] [0.6,266] 3
DRNL MOC efferent - latency (ms) maximum attenuation (dB) time constants (s) and weights BF-specific rate-to-attenuation factor applied to IC firing rate	10 35 [0.055 0.4 1] [0.9 0.1 0] [6e3 0 0]
Inner hair-cell (IHC) cilia /basilar membrane time constant (ms) basilar membrane/cilia displacement scalar maximum and resting conductance (nS) displacement sensitivity [s0 s1] (nm^{-1}) and offset [u0 u1] (nm)	1.2 0.01 6 0.1 [6 1] [0.3 1]
IHC - endocochlear potential Et and potassium reversal potential Ek (mV) potassium conductance Gk (nS) IHC capacitance Cab (pF.cm^{-2}) combined resistance Rpc (ohm.cm^{-2})	100 -80 21 1 0.04
IHC Pre-synaptic calcium current - reversal potential ECa (mV) channel opening parameters [βCa γCa] membrane time constant τM (μs) spontaneous-rate fiber types calcium clearance [low- medium- high-SR] time constants τCa (μs) [Ca^{2+}] ³ to probability scalar z maximum Ca^{2+} conductance (nS)	66 [400 100] 50 low, medium and high SR [80 120 200] 45e12 25
IHC-AN neurotransmitters (3-store model) – maximum vesicles available for release M rate of vesicle replenishment from depletion y (s^{-1}) and loss from the cleft l (s^{-1}) rate of vesicle reprocessing from re-uptake to ready-release pools x (s^{-1}) rate of vesicle re-uptake from cleft to cell r (s^{-1}) AN fiber refractory period (ms)	17 8 5 100 4 0.75
Brainstem 1st (CN) & 2nd (IC) order MacGregor chopper cells number of input AN/CN fibers per CN/IC cell and of CN cells per BF current per spike [CN IC] (nC) dendritic low-pass cutoff [CN IC] (Hz) membrane capacitance Cm (nF) potassium recovery time constant tauGk (ms) increment in conductance Gk after spike (μS) equilibrium threshold Th0 (mV) variable threshold tauTh and membrane time constant tauM (ms) potassium reversal potential Ek , resting potential Er and spike height Eb (mV)	10 10 [29 150] [50 100] 16.7 0.5 133 10 20 2 -10 -60 60

140

141 *Table 1. Parameters for the MAP (v.1_14j_2017) model of the normal auditory periphery.*

142

143 *Dynamic range analyses*

144 The role of the efferent system in DRA at the AN level was examined by comparing the
145 output of the encoder under four efferent conditions. These included the normal-hearing
146 condition ('normal') and conditions disabling the acoustic reflex ('noAR'), the MOCR
147 ('noMOCR') and both efferent reflexes ('noEff'). The parameters in the MAP model to create
148 different efferent-disabled conditions are described below:

149 (1) To disable the acoustic reflex in MAP, the parameters that determine the minimum
150 number of spikes to activate the reflex, was raised from 40 ('normal') to 10^6 spikes/sec so that no
151 attenuation was applied to the stapes displacement.

152 (2) To disable the MOCR, the DRNL parameter that determines the attenuation strength
153 applied to the basilar membrane displacement in the non-linear path of the DRNL module
154 (DNRLa) was changed from 1 ('normal') to 0, effectively deactivating the MOCR.

155 Based on physiological findings (e.g. Wen et al., 2009), RLFs exhibit DRA when firing
156 rates are probed at various levels along a continuous and silent-free stimulation that sets a
157 *context* level. We expected RLFs to shift closer to the context level when both efferent reflexes
158 are activated (under 'normal' simulation). Following the analyses in Wen et al. (2009), our
159 measures included RLFs, normalized RLFs, level at 50% of normalized RLFs, firing rate slope,
160 and sensitivity index δ' .

161 The RLFs were based on the mean firing at the BF and SR of interest, as a function of
162 probe level. The RLFs were fitted with a four-parameter logistic function:

163
$$R(L) = R_{min} + \frac{(R_{max} - R_{min})}{1 + \exp(-S \cdot (L - \theta_e))} \quad (\text{EQ.1})$$

164 where L is the input level; R_{min} and R_{max} are the minimum and the maximum firing rates,
165 respectively; θ_e is the response threshold in dB SPL; S is the slope of the RLF. The least-squared
166 method was used to determine the parameters. The firing rates under each condition were also
167 normalized between 0 and 1 using the following equation:

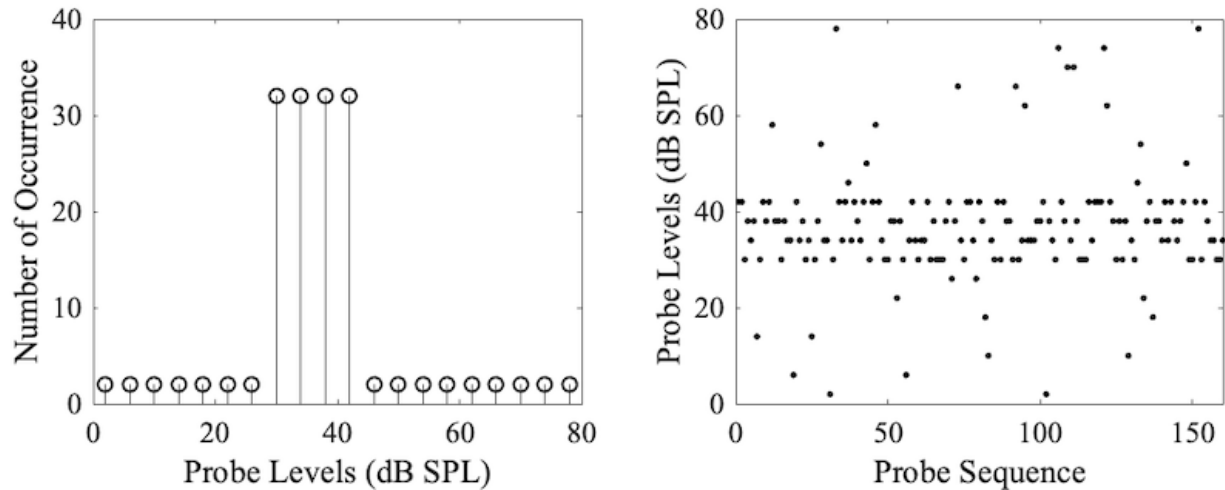
$$168 \quad R_{norm} = \frac{R - R_{min}}{(R_{max} - R_{min})} \quad (\text{EQ.2})$$

169 The horizontal shift of RLFs was quantified by measuring the increase in the threshold
170 parameter θ_e , the level at which the function reaches half its maximum. Wen et al. (2009) also
171 used rate slope and sensitivity index δ' to examine the impact of rate *variabilities* on the
172 precision of intensity coding along the RLF. The rate slope is the slope of the RLF at a given
173 probe level. Sensitivity index δ' , developed by Colburn et al. (2003), is defined as the ratio of the
174 rate slope to the standard deviation (SD) of the rates.

175 In order to observe the change of RLF shift under various efferent activation conditions,
176 three experimental paradigms were implemented and compared.

177 A 'baseline' paradigm was used to generate predictions of human RLFs without DRA.
178 This paradigm was similar to those traditionally used in small-mammal electrophysiological
179 studies, where a silent gap preceded each probe, thereby resetting efferent reflexes and hair cells
180 to resting states prior to each measure of firing rate. The probe signal was either a pure tone pip
181 (of frequency matching the fiber's BF) or a broadband noise burst, each 50 ms in duration, with
182 2-ms rise/fall times and preceded by a 200-ms silence. The probe level spanned 0 – 80 dB SPL
183 for tones and 20 – 100 dB SPL for broadband noise in 4-dB steps. At each probe level, the 50-ms
184 probe was processed through the encoder model, and the mean firing rates were averaged from
185 the activities of all 333 fibers of the same SR and BF.

186 A second paradigm emulated that employed by Dean et al. (2005) and Wen et al. (2009).
187 In each stimulus, a ‘high probability region’ (HPR) was specified where a range of probe levels
188 occurred more frequently than other probe levels throughout a continuous and silent-free
189 stimulation. The probe signals were the same tone pips or noise bursts as those used in the
190 baseline paradigm. This HPR paradigm differed from that of Wen et al. (2009) in that they used
191 continuous stimulation for 5 minutes, while the computational demands of the MAP model
192 limited our stimuli to 8 seconds. The probe levels (each 50 ms in duration, with 2-ms rise/fall
193 times) were randomly varied over the duration of stimulation, but the ongoing stimulation was
194 always dominated by a range of sound levels centered on a given context level. Specifically, the
195 probe level spanned 0 – 80 dB SPL for tones and 20 – 100 dB SPL for broadband noise in 4-dB
196 steps, but the probe levels inside the HPR occurred 80% of the time while the levels outside of it
197 occurred 20% of the time (Figure 2, left panel). The HPR mean levels were 36, 48, 60, and 72 dB
198 SPL for tonal stimulation and 48, 60, 72, and 84 dB SPL for noise stimulation. Within a
199 stimulation sequence, HPR levels spanned a 12-dB range. During our 8-second stimuli, 160 50-
200 ms probes were presented continuously, and probe levels were assigned in a pre-determined
201 random order (Figure 2, right panel). Ten continuous runs of different level randomizations were
202 completed for each of the four efferent conditions. As in the Wen et al. (2009) studies, the
203 response of a single fiber was recorded. The firing rate was averaged for each probe level and
204 across the ten runs (over a total of 20 occurrences per probe level).
205



206

207 *Figure 2. An HPR mean level of 36 dB: (Left) histogram of probe levels and (Right) example of*
 208 *probe level changes during a continuous, 8-second stimulation made of 160 x 50 ms pips/bursts.*

209

210 The ‘precursor’ paradigm was employed as a more computationally efficient alternative
 211 to the HPR paradigm. The processing of the HPR paradigm at a given HPR level requires a
 212 continuous and prolonged signal, usually hundreds of seconds, in order to present a randomized
 213 sequence of probe levels to a single fiber. A disadvantage of such processing is that measuring
 214 the activity of one fiber among thirty thousand does not make computationally efficient use of
 215 the MAP model. Instead, the precursor paradigm employs a steady precursor signal of set
 216 duration that immediately precedes a given probe level. For each combination of precursor and
 217 probe levels, firing rate is then computed over the 50 ms probe duration as the average firing rate
 218 of the 333 AN fibers of same BF and SR, thereby greatly improving computational efficiency. A
 219 similar approach is often used in psychophysical studies on the effects of efferent stimulation
 220 (e.g. Strickland, 2008). Here, the precursor duration was set long enough (400 ms, with 5 ms
 221 rise/fall times) that the modelled efferent reflexes fully stabilized. The 50-ms target probe was
 222 presented immediately after this precursor (with 2 ms rise/fall times). The precursor was the

223 same type of sound as the probe (i.e., tones of the same frequency or noises of the same
224 spectrum). The precursor levels were set to the same levels as the HPR paradigm mean levels,
225 following which the probe level was selected between 0 and 80 dB SPL for tones or 20 and 100
226 dB for noise (in 4-dB steps). As in the baseline paradigm, each 450-ms (precursor + probe)
227 combination was processed through the model independently.

228 *The MAPsim decoder*

229 The purpose of the decoder (right-hand section of Figure 1) in MAPsim is to invert the
230 encoding process and reconstruct the original input signal as well as the encoding stage will
231 allow. The role of the efferent reflexes in the efficient coding of sound can thus be studied
232 psychophysically from the quality of the reconstructed acoustic signal. There are two steps in the
233 decoding stage.

234 First, the decoder takes in the spike trains from the modelled AN fibers and feeds them
235 through a bank of gammatone filters (fourth order) centered on corresponding BFs to generate
236 wavelets (EQ.3):

$$237 \quad O_n(t) = \Gamma_n * I_n(t) \quad (\text{EQ.3})$$

238 where n is the BF channel index (1 to 30), t is time, Γ_n is the gammatone filter centered on the
239 channel n BF, $I_n(t)$ is the input AN spike train at time t in channel n , and $O_n(t)$ is the result of the
240 convolution between the input spike train and the gammatone filter (i.e. the resulting gammatone
241 wavelet train) at time t in channel n . Using this approach to decoding, the amplitude envelope of
242 the output waveform is largely determined by the spike rate (and hence the number of wavelets
243 at a given time), while the fine structure of the waveform is determined by the timing of the
244 action potentials (the average wavelet phase).

245 Second, the wavelet trains are summed across BFs and SRs, as follows. Since the brain
246 has access to efferent signals, we posit that it naturally incorporates them in its interpretation of
247 input signal level. Efferent signals are thus used to re-expand the signal, i.e. to invert most of the
248 compression the cochlear encoder had applied. To implement this re-expansion, the signal at
249 each BF is multiplied by the inverted MOCR attenuation, before summing wavelet trains across
250 BFs and finally multiplying the resulting signal by the inverted acoustic reflex attenuation. The
251 channel-specific, MOCR attenuation, $Att_n(t)$ and the broadband acoustic reflex attenuation,
252 $Att_b(t)$, both time-dependent, are extracted from the MAP model and expansion is implemented
253 according to EQ. 4:

$$254 \quad O(t) = \frac{\sum_{n=1}^{30} [O_n(t)/Att_n(t)]}{Att_b(t)} \quad (\text{EQ.4})$$

255
256 Finally, a spectral correction is applied to the reconstructed soundwave for its long-term
257 spectrum to match that of the MAPsim input soundwave. The scripts for the MAP model and the
258 decoder are available on request.

259 ***Psychophysical evaluation***

260 If the efferent system is key to DRA, the absence of the system will result in widespread
261 saturation of firing rates and drastically impair the ability to encode and recognize complex
262 spectro-temporal patterns, such as those of speech. Additionally, previous simulations using
263 automatic speech recognition have shown the potential improvement of speech intelligibility in
264 noise under efferent reflexes (Clark et al., 2012). Here, speech recognition in noise with human
265 subjects was used in a perceptual evaluation task to examine the role of efferent reflexes on
266 efficient coding of intensity. The importance of efferent reflexes in MAPsim output quality were
267 assessed through speech reception thresholds (SRTs) in noise. The experiment is designed to

268 measure the beneficial effects of the two compressive efferent reflexes working together. Since
 269 these reflexes both act to compress the dynamic range, compensating expansions were explored
 270 in order to improve the quality of the output. Since the reconstructed signal from the simulator
 271 represents the brain's interpretation of the stimulus, and the brain has access to the reflex signals,
 272 it is presumed that it can take them into account. The SRTs were obtained with young normal-
 273 hearing adults presented with stimuli that underwent different processing conditions (Table 2).
 274

	Efferent reflexes disabled	Efferent reflexes enabled		
	no eff.	no exp.	MOC exp.	MOC*AR exp.
MOC-based expansion	X	X	✓	✓
AR-based expansion	X	X	X	✓

275
 276 *Table 2. Expansion applied under each experimental condition for the processed conditions.*

277
 278 To assess the importance of efferent-based expansion at the decoding stage, with efferent
 279 reflexes enabled at the encoding stage, three conditions applied different amounts of expansion.
 280 The first applied no expansion to the output of EQ. 3 (called 'no exp.'). The second applied only
 281 the EQ. 4 MOCR expansion (called 'MOCR exp.'). The third applied both (EQ.3 and EQ.4)
 282 acoustic reflex and MOCR expansions (called 'MOCR*AR exp.'). A control condition
 283 ('unproc.') employed the unprocessed, original stimuli. The condition applying the full
 284 expansion ('MOCR*AR exp.') was expected to yield SRTs closest to those obtained with
 285 unprocessed stimuli, which, if close enough, would constitute a validation of MAPsim. To
 286 demonstrate the importance of efferent reflexes, a final condition had both reflexes disabled at

287 the encoding stage (called 'no eff.'). Since efferent reflexes were disabled, no expansion was
288 applied in this condition. SRTs for the 'no eff.' condition were compared to those for the
289 'MOC*AR exp.' and 'unproc.' conditions to measure the impact of knocking out efferent reflexes.

290 Twelve young adults with self-assessed normal hearing (17-31 years old, mean 22 years
291 old) were recruited from the Cardiff University undergraduate population to perform the SRT
292 task. All participants were briefed in writing and verbally before signing a consent form. All
293 testing and forms complied with the ethical rules of the Cardiff University School of Psychology
294 Institutional Review Board.

295 SRT measurements employed a digit-triplet recognition task. Each stimulus comprised of
296 a 400-ms precursor followed by three non-repeating, randomly selected digits from 0 to 9
297 (except disyllabic digit 7) uttered by a British female, each centered within a 700-ms audio file.
298 The precursor was steady-state noise spectrally colored to the female voice, which set the
299 stimulus context level and allowed the efferent reflexes of the MAP model to stabilize. The
300 masker was the same speech-shaped noise as the precursor noise.

301 SRTs were measured using a one-down-one-up adaptive procedure. In each run, the
302 signal-to-noise ratio (SNR) started with the digits being highly intelligible (at 0 dB SNR) and
303 decreased by a step size of 4 dB as long as correct responses were given. After the first reversal,
304 the step size was reduced to 2 dB. Correct recognition of two or three digits in the correct
305 positions was scored a correct response. Recognition of one or zero digits was scored an
306 incorrect response. The overall level of the speech and the noise mixed was maintained at 65 dB
307 SPL, both at the input and the output of the simulator. Each run stopped when 10 reversals were
308 reached, and the SNRs of all trials over the last 8 reversals were averaged to compute the SRT of
309 that run. The SRT was taken as the average over 3 runs under each condition. Before testing, one

310 practice run using unprocessed stimuli was given to the participants to familiarize them with the
311 task. The practice run was also used to screen for unsuspected participant hearing impairment.
312 The entire experiment took about 1 hour to complete. Participants received payment at the end of
313 the experiment. Repeated-measure analysis of variance was conducted for the SRTs in the IBM
314 SPSS software (version 26.0).

315 **RESULTS**

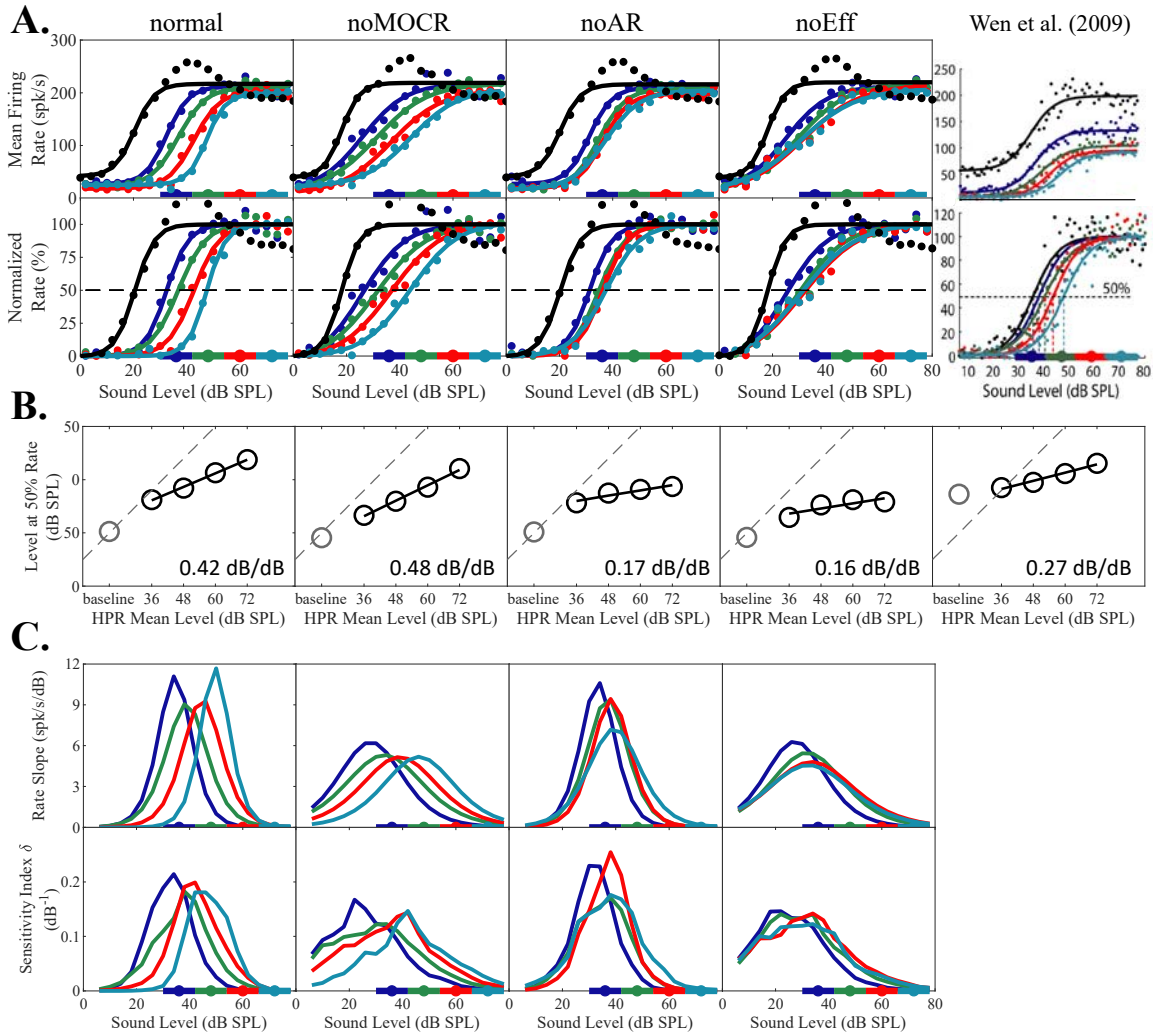
316 First, the model was used to simulate auditory nerve responses for two cases: baseline *vs.*
317 HPR using tones, and baseline *vs.* HPR using broadband noise. These cases are compared with
318 those from Wen et al. (2009) from their Figures 2 and 4, respectively, so we use simulated nerve
319 fibers that are matched in best frequency and spontaneous rate with the fibers they observed.
320 Second, the results of the precursor paradigm were compared to those of the HPR paradigm
321 using tones to verify that the outcomes were similar. The precursor paradigm was also used to
322 show the responses of the auditory nerves of different spontaneous rates presented with various
323 types of stimuli. Third, the results of the speech-in-noise test were compared under deactivation
324 *vs.* full activation of efferent reflexes and with varying amounts of expansion when efferent
325 reflexes were activated. The validation outcome of the simulator is also reported in this section.

326 ***Dynamic range adaptation through the HPR paradigm***

327 Figure 3 shows the average responses of a high SR fiber whose BF matched the probe
328 tone frequency, comparing baseline and HPR-paradigm conditions. The rightmost column shows
329 the physiological data of Wen et al. (2009) collected from a cat fiber responding to 550-Hz tones.
330 The rest of the data were from a simulated high-SR human fiber responding to 580-Hz tones

331 under ‘normal’ (leftmost column), ‘noMOCR’ (second left column), ‘noAR’ (middle column), and
 332 ‘noEff’ (second right column) processing conditions.

333



334

335 *Figure 3. Response of a high SR fiber (BF = 580 Hz) to 580-Hz tones. From left to right panels:*
 336 *modeled human data for normal, noMOCR, noAR and noEff conditions, and Cat*
 337 *electrophysiological data (BF = 550 Hz, tone at 550 Hz, from Figure 2 of Wen et al., 2009,*
 338 *adapted with permission, Copyright © 2009 Society for Neuroscience). Different colored*
 339 *symbols and lines are data points and fitted curves for different HPR levels, indicated by colored*

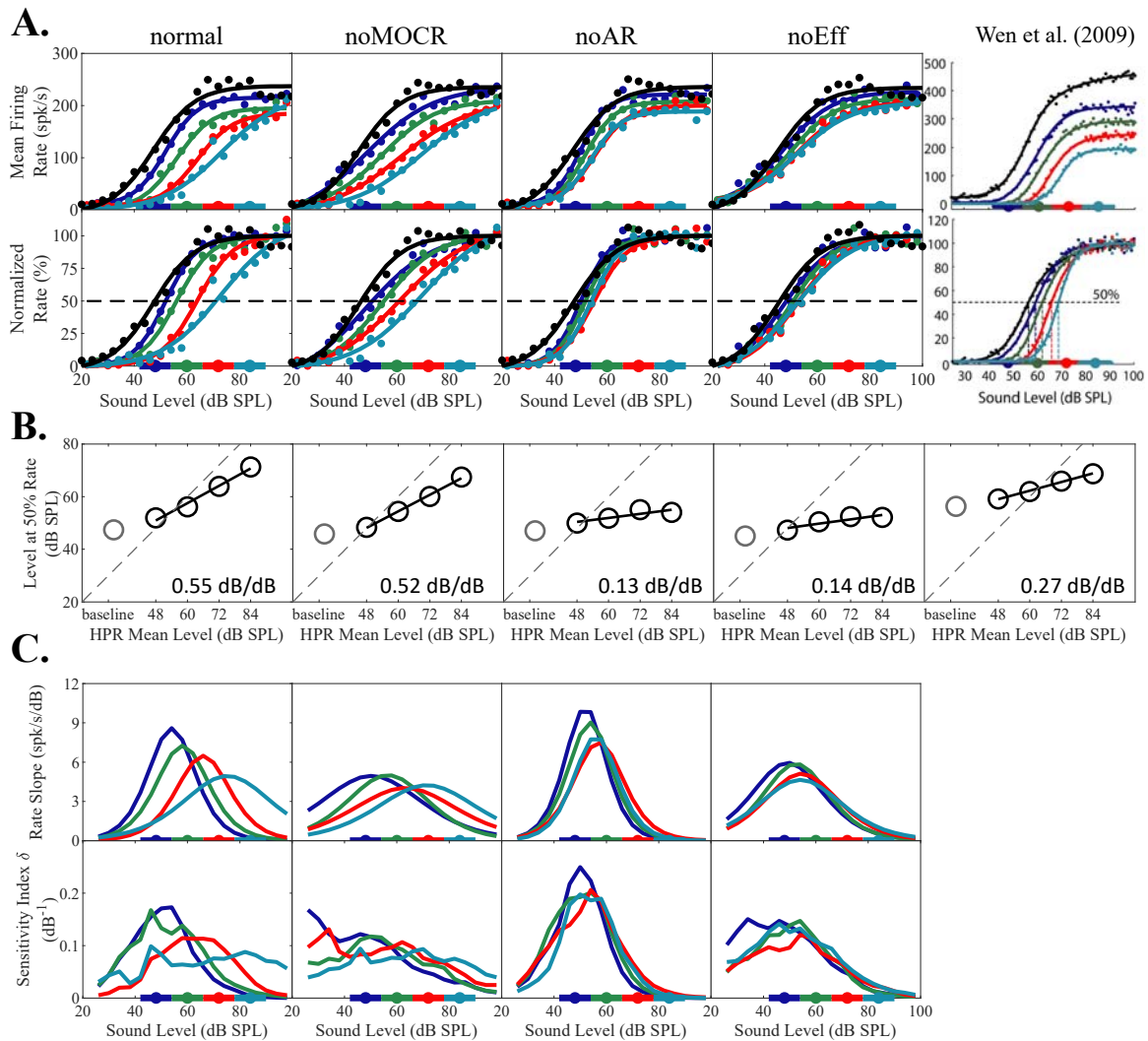
340 segments on the x-axis, while black is the baseline condition (with no DRA). A: RLFs (top) and
341 normalized RLFs (bottom). B: level at 50% rate. C: rate slope (top) and sensitivity index δ'
342 (bottom).

343 Under 'normal' condition, the RLFs shift toward the right with increasing HPR levels
344 (Figure 3A), a DRA that was observed in the physiological data. Classical firing rate adaptation,
345 the decrease of the maximum firing rate with increasing HPR level, is minimal in the simulation,
346 but when the RLFs are normalized for maximum firing rate (second row of panels), there is
347 greater DRA than in the physiological data. The 50% point shifts by 0.42 dB per dB change in
348 HPR level for the modeled data, and only by 0.16 dB/dB for the physiological data. As HPR
349 level increases, there is also a clear rightward shift in the peak rate slope and the peak sensitive
350 index δ' in the 'normal' condition.

351 DRA is present under 'noMOCR' condition and reaches 0.48 dB/dB. However, the rate
352 slope and sensitive index δ' of 'noMOCR' are shallower compared to 'normal', suggesting a
353 reduction of sensitivity in encoding intensity change. On the other hand, 'noAR' shows a
354 drastically reduced DRA with HPR levels compared to 'normal' or 'noMOCR' conditions,
355 reaching only 0.17 dB/dB. The absence of acoustic reflex does not affect the sensitivity of
356 intensity change coding as its sensitivity indices are comparable to those of 'normal'. Finally, the
357 absence of both acoustic reflexes (i.e., 'noEff') shows combined effects of severe reduction, but
358 not an eradication, of DRA.

359 Figure 4 shows modeling of the second fiber type measured by Wen et al. (2009): the
360 average response of a medium-SR fiber to broadband noise in the baseline and the HPR
361 paradigm conditions. The BF of the modeled human fiber was selected at 1280 Hz to best match
362 the 1300 Hz BF of the Cat fiber. Overall, the results using noise and a medium-SR fiber are

363 similar to those observed for tones with a high SR fiber, but with two small differences. First, the
 364 maximum firing rate decreases more markedly with increasing HPR level. Second, the amount of
 365 DRA is larger for noise than for tones, which is 0.55 and 0.52 dB/dB for ‘normal’ and ‘noMOCR’
 366 under noise stimulation, respectively.
 367



368
 369 *Figure 4. As figure 3, but for a medium SR fiber ($BF = 1280$ Hz) responding to broadband noise.*
 370

371 **Precursor paradigm shown as a more efficient alternative to HPR paradigm**

372 The results of the precursor paradigm are similar to those of the HPR paradigm (Figure 5).

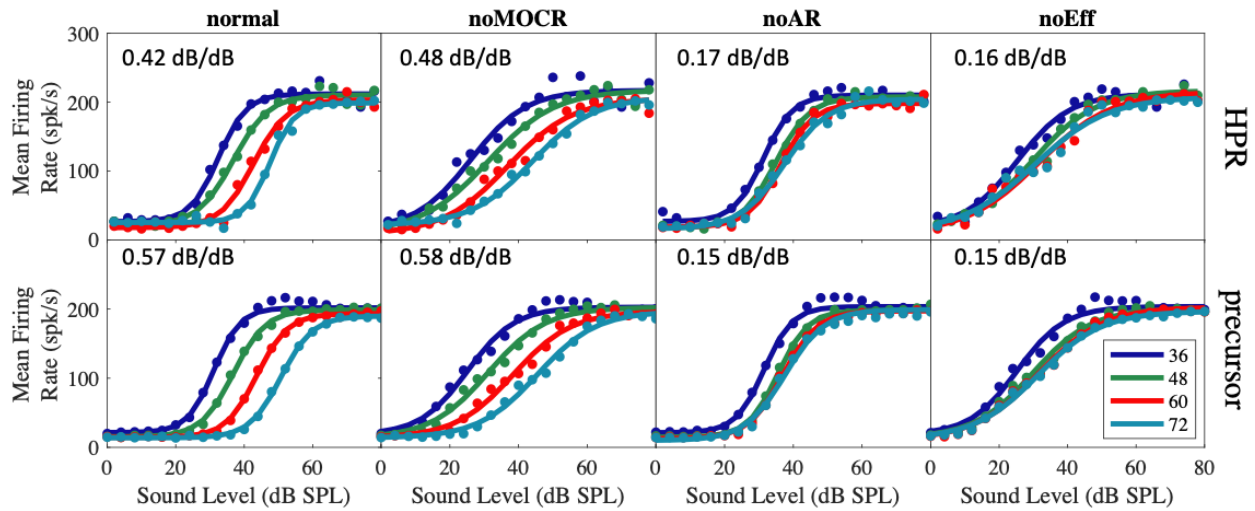
373 With the precursors, the normal RLFs show rightward shift with increasing precursor level, and

374 the amount of such DRA is slightly larger than that of the HPR level, yielding 0.57 dB/dB shift

375 for HSR fibers with 580-Hz BF responding to tones at the BF. The deactivation of efferent

376 reflexes reduces DRA to 0.15 dB/dB.

377



378

379 *Figure 5. RLFs of high-SR fibers (BF 580 Hz) to 580-Hz tones under different paradigms,*

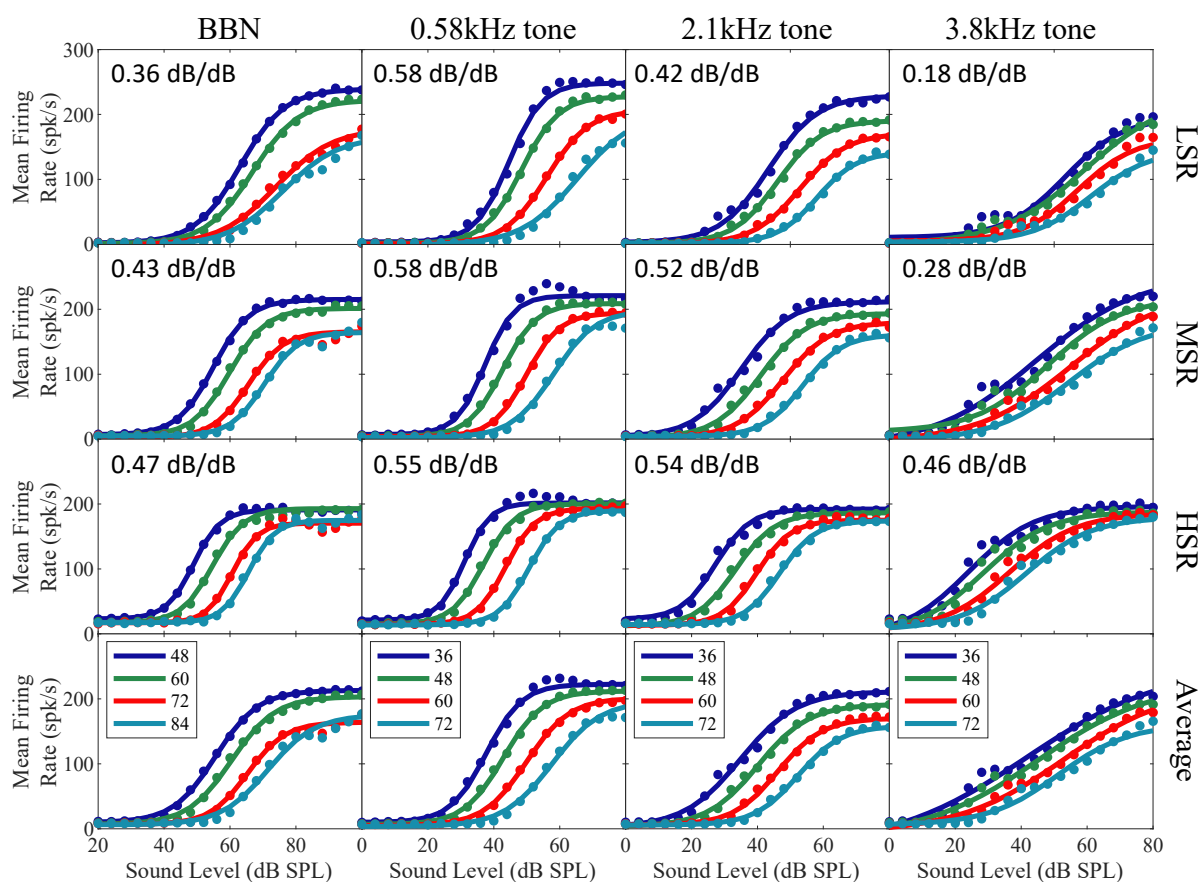
380 *hearing conditions and context levels. From left to right panels: modeled human data for normal,*

381 *noMOCR, noAR and noEff conditions. Top panels: HPR paradigm. Bottom panels: precursor*

382 *paradigm. Dotted lines: RLFs with context levels in the 36-72 dB range. Solid lines: logistic fits*

383 *of predicted RLFs. Top left of each panel: DRA (dB/dB).*

384



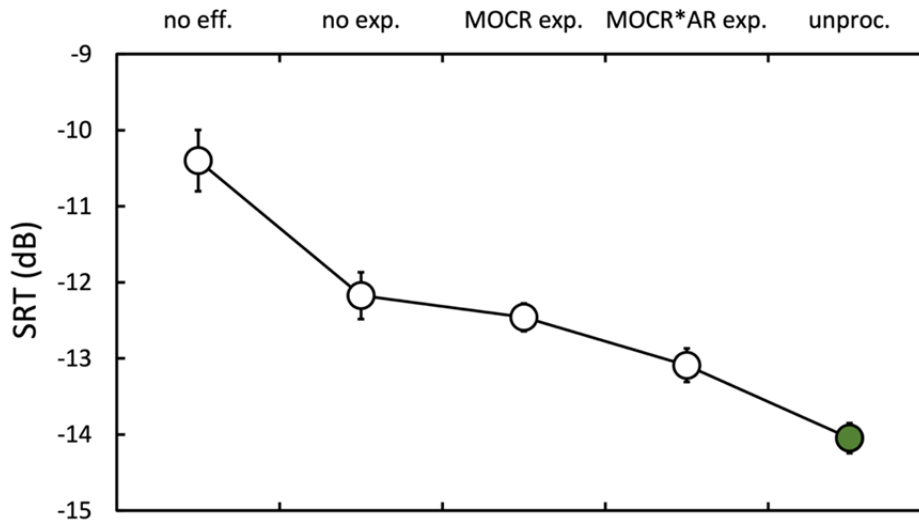
385
 386 *Figure 6. RLFs for model AN fibers of different SRs for broadband noise (BBN) or tones. From*
 387 *left to right panels: BF = 1 kHz, noise stimuli; BF of 580 Hz, 2.1 kHz and 3.8-kHz with*
 388 *matching-frequency tone stimuli. Top to bottom panels: low, medium- and high-SR fibers, and*
 389 *average responses of fibers of the three spontaneous rates.*

390
 391 Analysis of normal fibers responding to various types of stimuli (noise and tones of
 392 different frequencies) was performed for each spontaneous rate class using the precursor
 393 paradigm. The results (Figure 6) show that (1) RLFs tend to saturate at lower probe levels for
 394 fibers with high SR than for fibers with low SR regardless of the stimulus frequencies, but robust
 395 DRA occurs for fibers of all three SRs, (2) the amount of DRA decreases with increasing tone

396 frequency, especially for low-SR fibers, and (3) the amount of DRA increases with fibers' SRs
397 for high-frequency tones, but the effect is not obvious for low-frequency tones.

398 *Efferent reflexes in the efficient encoding of speech*

399 Figure 7 shows the SRTs (signal-to-noise ratio for 50% digits correctly reported)
400 achieved by listeners attending to the MAPsim output. Intelligible speech was thus heard using
401 each simulation, but SRTs were improved by including certain features in the simulation.
402



403
404 *Figure 7. Digit-triplet SRTs obtained from listeners attending to the original signal (unproc.)*
405 *and MAPsim outputs with efferent reflexes disabled (no eff.), with them enabled but without*
406 *expansion (no exp.) and with expansion based on inverted efferent signals (MOCR exp. and*
407 *MOCR*AR exp.). Error bars are standard errors of means.*

408

		Mean Difference	SE	<i>p</i>
no eff.	no exp.	1.773*	0.410	0.012
	MOCR exp.	2.059**	0.452	0.008
	MOCR*AR exp.	2.689**	0.299	0.001
	unproc.	3.647**	0.509	0.001
no exp.	MOCR exp.	0.286	0.265	1.000
	MOCR*AR exp.	0.916	0.356	0.260
	unproc.	1.873**	0.376	0.004
MOCR exp.	MOCR*AR exp.	0.630	0.308	0.657
	unproc.	1.587**	0.222	0.001
MOCR*AR exp.	unproc.	0.958	0.343	0.176

409

410 *Table 3. Post hoc pairwise comparisons between MAPsim processing conditions. Adjustment for*
411 *multiple comparisons: Bonferroni. *: $p < 0.05$. **: $p < 0.01$.*

412

413 The importance of compensating for the peripheral compression introduced by the MAP
414 model was evaluated. The SRTs of ‘no exp.’ (neither expansion applied), ‘MOCR exp.’ (MOCR
415 expansion only), ‘MOCR*AR exp.’ (both expansions applied), and ‘unproc.’ (original,
416 unprocessed stimuli) were compared (Table 3). The mean thresholds were progressively reduced
417 by adding compensation for the MOCR and then the MOCR and AR, with deficit compared to
418 the unprocessed case reaching less than one dB. However, they did not improve significantly
419 over the ‘no exp.’ case.

420 The role of efferent reflexes in coding speech in noise was examined by comparing ‘no
421 eff.’ to ‘MOCR*AR exp.’ and ‘unproc.’ conditions. Under ‘no eff.’, efferent reflexes were
422 deactivated in the MAP model, hence no expansion was applied. The results show that when
423 efferent reflexes are absent, the SRT increases significantly, elevating nearly 2.7 dB from that of
424 ‘MOCR*AR exp.’, $p < 0.001$, and 3.6 dB from that of ‘unproc.’, $p < 0.001$.

425 **DISCUSSION**

426 The modeling based on the MAP model (Panda et al., 2014), shows how DRA may occur at
427 sound levels up to at least 72 dB, such that the system can remain mostly saturation-free and
428 efficiently transmit to the brain information about temporal modulations of speech uttered at
429 normal levels. Specifically, DRA is brought about by two efferent feedback loops: the acoustic
430 reflex shifts RLFs with context level, by attenuating transmission through the middle ear; the
431 MOCR works in parallel with the acoustic reflex by modulating the electromotility of the outer
432 hair cells, fine-tuning the slope of the RLFs to ensure optimal and precise encoding of sound
433 intensity. Compared to the Wen et al. data, the MAP model predicts a greater effect of DRA but
434 much smaller classical adaptation effects. Greater DRA results from the inclusion of the two
435 efferent processes, which were suppressed by anesthesia in the physiological work. Reduced
436 classical adaptation may come from the use of much shorter HPR stimuli (8 seconds, compared
437 to 5 minutes) in our study, combined with a model that, in any case, only simulates short-term
438 adaptation.

439 After decoding the firing patterns predicted by MAP back into an acoustic signal, speech
440 recognition in noise through MAPsim significantly improves with activated efferent reflexes,
441 illustrating the role of efferent reflexes in efficient coding of speech, which is a signal highly
442 modulated in spectral and temporal domains (Drullman et al., 1994).

443 *Mechanisms of dynamic range adaptation in AN fibers*

444 The shifting of RLFs toward higher levels as context level increases was first shown in
445 animal studies at the auditory nerve (Wen et al., 2009) and the inferior colliculus (Dean et al.,
446 2005, 2008) levels. Many adaptive properties of the AN are associated with the synapses
447 between inner hair cells and fibers (Moser and Beutner, 2000; Goutman and Glowatzki, 2007),
448 inspiring auditory modeling scientists to simulate DRA through changing the dynamics of inner-
449 hair-cell-auditory-nerve synapses. Zilany & Carney (2010) have successfully simulated DRA by
450 implementing power-law dynamics at the junction between inner hair cells and fibers in their
451 auditory model. However, it is unclear whether these power-law dynamics are physiologically
452 plausible. The current study suggests that DRA at the AN could originate from the efferent
453 reflexes, especially the AR, which would not be evident from studies with anesthetized small
454 mammals. Interestingly, anesthetized animals still show DRA at higher centers (Dean et al. 2005,
455 2008), suggesting that other mechanisms are also at work at these levels of the nervous system.

456 The MAP model predicts that the MOCR and the acoustic reflex take on different roles in
457 DRA. The modeled MOCR receives contributions from the AN fibers of all three spontaneous
458 rates. When disabling the MOCR, the slope of the RLF decreases, suggesting that the auditory
459 system becomes less sensitive to sound intensity change. In other words, a slight change in sound
460 intensity does not induce as much difference in the firing rates in the absence of MOCR as in the
461 normal condition. On the other hand, the acoustic reflex is activated only at high intensities to
462 attenuate the stapes displacement, and the amount of attenuation solely depends on the output
463 from the stream that involves the low-SR fibers. When the acoustic reflex is disabled, the firing
464 rates at high probe levels are no longer suppressed, causing the RLFs of the higher context levels
465 to shift leftward and overlap with the RLFs of the lower context levels. Therefore, the absence of

466 acoustic reflex impacts the sensitivity and accuracy of intensity coding at higher context levels
467 and the auditory system's ability to perform DRA efficiently.

468 The efferent reflexes have been suggested as a source of DRA but their role could not be
469 examined in small mammals because anesthesia in physiological studies at least partially
470 suppresses the efferent system. Note that, in the current study, when efferent reflexes are
471 activated, the amount of DRA far exceeds what has been found in physiological studies,
472 suggesting that the contribution of efferent reflexes to DRA was obscured under anesthesia but
473 can be revealed using computational modeling.

474 Some DRA remained in both modeled and empirical data, even with both efferent
475 reflexes disabled, suggesting an additional source of adaptation in the peripheral auditory system.
476 The most plausible explanation for this remaining adaptation resides in the dynamics of
477 neurotransmitter vesicle release into the cleft, replenishment within the inner hair cell and
478 reuptake by the hair cell from the cleft, as emulated by the 3-store model (Meddis, 1986, in its
479 probabilistic implementation, and Sumner et al., 2002, in the quantized implementation used in
480 this study). While such depletion accounts for some firing-rate adaptation, the presence of DRA
481 with deactivated efferent reflexes shows that non-efferent-related DRA is an emergent property
482 of the 3-store hair cell model.

483 *Classical adaptation in AN fibers*

484 Figure 6 shows some evidence of classical adaptation, but mainly in the low SR fibers
485 and much less than seen throughout the Wen et al. data. Firing-rate adaptation occurs on
486 different timescales. Short timescales (a few milliseconds or tens of milliseconds) are expressed
487 in the 3-store model via fast available-store depletion but long-term firing-rate adaptation (Kiang
488 et al., 1965) is not. Long-term adaptation may stem from a gradual decrease, under steady

489 stimulation, of the ion flux (Strimbu et al., 2019) required by inner hair cells to drive
490 neurotransmitter release into the cleft. It is not captured in the MAP model and therefore not in
491 our predictions. The HPR paradigm used in Wen et al. (2009) may capture such adaptation in
492 high SR fibers because the stimulus is minutes in duration (see Figures 3 and 4).

493 The model predicts differences in short-term adaptation as a function of spontaneous rate
494 (Figure 6) due to differences in the time constant τ_{Ca} , which reflects the dwell time of presynaptic
495 calcium in the vicinity of the synapse and therefore determines the release characteristics of the
496 synapse. At saturation, despite high depletion of the available store, the probability of release of
497 vesicles is much higher in high-SR than in low SR-fibers, such that short-term firing-rate
498 adaptation of high-SR fibers is limited in the HPR or precursor paradigms.

499 ***The precursor paradigm***

500 The precursor paradigm significantly improves the efficiency of setting up the context
501 level compared to the HPR paradigm. The precursor precedes the probe with an identical signal
502 that is 400-ms long and sets the context level. The precursor allows sufficient time to activate the
503 efferent system to produce a given level of DRA. The precursor paradigm performed
504 equivalently to the HPR paradigm in revealing DRA. Importantly, signals could be processed
505 much more efficiently under the precursor paradigm so that the roles of efferent reflexes could
506 be studied with perceptual measures using MAPsim. The equivalence of the HPR and precursor
507 paradigms is reassuring given that psychophysical studies generally employ the latter when
508 attempting to activate the efferent system.

509 ***Future use of the MAPsim simulator***

510 MAPsim provides a new simulation framework for efficiently exploring peripheral
511 auditory physiology, its pathologies and the corresponding perceptual impacts. Since all hearing

512 depends upon the signal encoded on the AN, the decoded sound will reflect any loss of
513 information occurring within the model of peripheral transduction and thus the effects of
514 modeled pathologies. MAPsim proved successful in that SRTs at the simulator validation stage
515 differed from those obtained with unprocessed stimuli by just 1 dB, suggesting very limited
516 information loss when simulating normal hearing.

517 MAPsim could serve as a powerful tool to simulate perceptual effects of specific hearing
518 pathologies, such as loss of inner vs. outer hair cells, loss of endocochlear potential and
519 synaptopathy. The present simulations enable us to see via psychophysical measures that a
520 deficient caudal efferent system could cause unrecoverable information loss and severely impair
521 the ability to recognize speech in steady-state noise. Previously, the role of the efferent system,
522 especially the MOCR, on speech recognition in noise was only studied through coupling the
523 MAP model with an artificial observer, such as an automatic speech recognition system (Clark et
524 al., 2012; Yasin et al., 2020), or through correlational studies where speech performance was
525 examined under different levels of efferent activation (Mertes et al., 2018). Here, the simulator
526 indicates specific effects of both MOCR and AR on human speech reception thresholds.

527 ***Conclusion***

528 Our findings confirm the potential of efferent reflexes to maintain DRA and enable
529 efficient coding of speech at the auditory nerve level. The MAP model predicts that the acoustic
530 reflex shifts the dynamic range of auditory-nerve fibers towards contextual levels and the MOC
531 reflex increases fiber sensitivity around that level. Our MAPsim simulator was validated for
532 normal hearing of speech stimuli. Being based on MAP, MAPsim can be used to simulate
533 specific sensorineural pathologies, opening the door to establishing their psychophysical
534 signatures, such that they may be differentially diagnosed.

535

REFERENCES

- 536 Chimento TC, Schreiner CE (1991) Adaptation and recovery from adaptation in single fiber
537 responses of the cat auditory nerve. *J Acoust Soc Am* 90:263–273.
- 538 Clark NR, Brown GJ, Juergens T, Meddis R (2012) A frequency-selective feedback model of
539 auditory efferent suppression and its implications for the recognition of speech in noise. *J*
540 *Acoust Soc Am* 132:1535–1541.
- 541 Colburn HS, Carney LH, Heinz MG (2003) Quantifying the information in auditory-nerve
542 responses for level discrimination. *JARO - J Assoc Res Otolaryngol* 4:294–311.
- 543 Dean I, Harper NS, McAlpine D (2005) Neural population coding of sound level adapts to
544 stimulus statistics. *Nat Neurosci* 8:1684–1689.
- 545 Dean I, Robinson BL, Harper NS, McAlpine D (2008) Rapid neural adaptation to sound level
546 statistics. *J Neurosci* 28:6430–6438.
- 547 Drullman R, Festen J, Plomp R (1994) Effect of temporal envelope smearing on speech reception.
548 *J Acoust Soc Am* 95:1053–1064.
- 549 Goutman JD, Glowatzki E (2007) Time course and calcium dependence of transmitter release at
550 a single ribbon synapse. *Proc Natl Acad Sci U S A* 104:16341–16346.
- 551 Guinan JJ, Gifford ML (1988) Effects of electrical stimulation of efferent olivocochlear neurons
552 on cat auditory-nerve fibers. I. Rate-level functions. *Hear Res* 33:97–113.
- 553 Harris DM, Dallos P (1979) Forward masking of auditory nerve fiber responses. *J Neurophysiol*
554 42:1083–1107.
- 555 Hung IJ, Dallos P (1972) Study of the acoustic reflex in human beings. I. Dynamic
556 characteristics. *J Acoust Soc Am* 52:1168–1180.
- 557 Kiang NY, Watanabe T, Thomas EC, Clark LF (1965) Discharge patterns of single fibers in the

558 cat's auditory nerve. MIT Press.

559 Liberman MC (1978) Auditory-nerve response from cats raised in a low-noise chamber. *J Acoust*
560 *Soc Am* 63:442–455.

561 Lopez-Poveda EA, Meddis R (2001) A human nonlinear cochlear filterbank. *J Acoust Soc Am*
562 110:3107–3118.

563 MacGregor RJ (1987) *Neural and Brain Modeling*. Academic Press.

564 Meddis R (1986) Simulation of mechanical to neural transduction in the auditory receptor. *J*
565 *Acoust Soc Am* 79:702–711.

566 Meddis R, Lecluyse W, Clark NR, Jürgens T, Tan CM, Panda MR, Brown GJ (2013) A
567 computer model of the auditory periphery and its application to the study of hearing. In:
568 *Advances in Experimental Medicine and Biology*, pp 11–20.

569 Mertes IB, Wilbanks EC, Leek MR (2018) Olivocochlear Efferent Activity is Associated With
570 the Slope of the Psychometric Function of Speech Recognition in Noise. *Ear Hear* 39:583–
571 593.

572 Moser T, Beutner D (2000) Kinetics of exocytosis and endocytosis at the cochlear inner hair cell
573 afferent synapse of the mouse. *PNAS* 97:883–888.

574 Panda MR, Lecluyse W, Tan CM, Jürgens T, Meddis R (2014) Hearing dummies: Individualized
575 computer models of hearing impairment. *Int J Audiol* 53:699–709.

576 Smith RL (1979) Adaptation, saturation, and physiological masking in single auditory-nerve
577 fibers. *J Acoust Soc Am* 65:166–178.

578 Smith RL, Zwislocki JJ (1975) Short-term adaptation and incremental responses of single
579 auditory-nerve fibers. *Biol Cybern* 17:169–182.

580 Strickland EA (2008) The relationship between precursor level and the temporal effect. *J Acoust*

581 Soc Am 123:946–954.

582 Strimbu CE, Prasad S, Hakizimana P, Fridberger A (2019) Control of hearing sensitivity by
583 tectorial membrane calcium. *Proc Natl Acad Sci U S A* 116:5756–5764.

584 Sumner CJ, Lopez-Poveda EA, O’Mard LP, Meddis R (2002) A revised model of the inner-hair
585 cell and auditory-nerve complex. *J Acoust Soc Am* 111:2178.

586 Watkins P V., Barbour DL (2008) Specialized neuronal adaptation for preserving input
587 sensitivity. *Nat Neurosci* 11:1259–1261.

588 Wen B, Wang GI, Dean I, Delgutte B (2009) Dynamic range adaptation to sound level statistics
589 in the auditory nerve. *J Neurosci* 29:13797–13808.

590 Winter IM, Robertson D, Yates GK (1990) Diversity of characteristic frequency rate-intensity
591 functions in guinea pig auditory nerve fibres. *Hear Res* 45:191–202.

592 Yasin I, Drga V, Liu F, Demosthenous A, Meddis R (2020) Optimizing Speech Recognition
593 Using a Computational Model of Human Hearing: Effect of Noise Type and Efferent Time
594 Constants. *IEEE Access* 8:56711–56719.

595 Young ED, Sachs MB (1979) Representation of steady-state vowels in the temporal aspects of
596 the discharge patterns of populations of auditory-nerve fibers. *J Acoust Soc Am* 66:1381–
597 1403.

598 Zilany MSA, Carney LH (2010) Power-Law Dynamics in an Auditory-Nerve Model Can
599 Account for Neural Adaptation to Sound-Level Statistics. *J Neurosci* 30:10380–10390.

600